Molecular Simulation of Adsorption of HCFC-22 in Pillared Clays

Qingyuan Yang, Xinping Bu, Chongli Zhong, and Yi-gui Li
Dept. of Chemical Engineering, Key Laboratory for Nanomaterials of Ministry of Education, Beijing University of Chemical Technology, Beijing 100029, China

DOI 10.1002/aic.10337
Published online in Wiley InterScience (www.interscience.wiley.com).

An extensive grand canonical Monte Carlo (GCMC) simulation combined with quantum mechanics calculations has been conducted to investigate the dependency of the adsorption isotherms, local density profiles, and orientational behaviors of HCFC-22 confined in pillared clays on pore width, porosity, pressure, and the density of the activated sites at 300 K. The calculated results suggest that there are optimal pore width and pressure for adsorption, and the effects of porosity and the activated sites on adsorption are significant at low pressure and become weaker with increasing pressure. A combination of the GCMC simulation and the quantum mechanics calculation results shows that hydrogen atom is the adsorption site of an HCFC-22 molecule adsorbed on the pillared clay walls and most of the molecules in the contact layers orient perpendicularly to the walls in the direction of C → H when physical adsorption is predominant, and the orientation changes with increasing pressure. © 2004 American Institute of Chemical Engineers *AIChE J,* 51: 281–291, 2005
Keywords: adsorption, molecular simulation, quantum mechanics, pillared clay, HCFC-22

Introduction

HCFC-22 ($CHClF_2$) is a typical substance among hydrochlorofluorocarbons (HCFCs), which has generally been accepted as the most suitable refrigerant for air conditioners and refrigerators. However, because of its potential for ozone depletion and greenhouse effects, it is a controlled transit substance. According to the Montreal protocol, HCFC-22 has to be phased out by the year 2030 for developed countries and 2040 for developing countries. It is thus an urgent task to search environmentally friendly alternatives to refrigerant HCFC-22. Tremendous studies have been reported in the literature.[1] Evidently, for the protection of the world's environment, the emission of organic vapors containing HCFC-22 in process vent gases needs to be controlled, and thus its recovery and recycling become an important issue.

Correspondence concerning this article should be addressed to C.-l. Zhong at zhongcl@mail.buct.edu.cn or zhongcl88@yahoo.com.

Among many technologies used for the capture and recovery of organic compound vapors, the adsorption process is perhaps the most common method.[2] Pillared clay, as a porous catalytic material similar to zeolite-based catalysts, has shown high catalytic activity for many industrial processes. Because the available interior pore volume of pillared clays is controlled by the distance between the opposite solid walls as well as the distribution of pillars, they have also been suggested experimentally as a new class of adsorbent for the processes of gas adsorption and separation.[3,4]

Molecular simulation is a powerful method to give deep insight into the phenomena studied at the molecular level,[5,6] which can offer references for the design of adsorption materials and the determination of optimum process conditions. Many papers have been published on the adsorption of simple fluids in pillared materials by molecular simulation methods. Cracknell et al.[7] used the grand canonical Monte Carlo (GCMC) method to study the adsorption isotherms and the heat of adsorption of inert gases in pillared clays. Yi et al.[8] studied the adsorption equilibria and diffusion of simple Lennard–

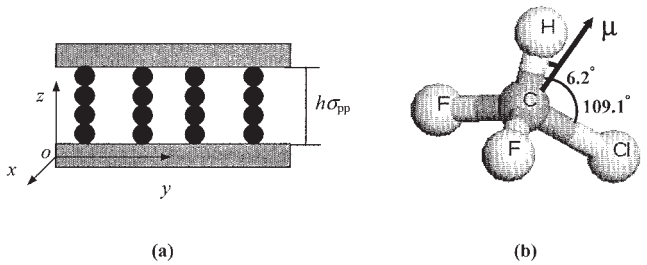

Figure 1. (a) Side view of the pillared clay, with pore width $H = h\sigma_{pp}$. σ_{pp} is the pillar atom size, h is the number of atoms composing one pillar; here $h = 4$; (b) representation of the orientation of dipole moment μ in HCFC-22 molecule.

Jones gas molecules in pillared clays by using both GCMC and molecular dynamics (MD) methods. Later, using the equilibrium molecular dynamics (EMD) method, the adsorption of some gases and their binary mixtures in pillared clays were also reported by this group.[9,10] More recently, Cao and Wang[11] investigated the adsorption behavior of carbon tetrachloride (CCl_4) in layered pillared pores.

It is noticed that the surface chemistry of adsorbents also plays an important role in adsorption capacity.[1] Some papers have also been published about the effects of surface chemistry on adsorption behavior in slit pores by molecular simulation methods.[12,13] Volpe and Cleri[14] and Smith et al.[15] studied the role of surface chemistry for hydrogen adsorption in single-wall carbon nanotubes.

Dipolar forces are essentially omnipresent in nature and play a prominent role in various chemical processes. Although investigations on dipolar fluids have been performed both experimentally and theoretically, such as the adsorption of water in a series of pillared clays has been investigated experimentally,[16-19] and molecular simulations have also been carried out to study its adsorption behaviors and microstructures in mineral clays,[20-22] there has not been, as far as we know, a related paper published on the adsorption simulation of dipolar fluids in pillared clays. In this work, HCFC-22 is modeled as a dipolar fluid, and its adsorption in pillared clays at ambient temperature $T = 300$ K was studied using the GCMC method combined with quantum mechanics calculations. The purpose of our work is to explore the dependency of adsorption and orientational behavior of HCFC-22 on the pore width, porosity, operational pressure, and surface chemistry of pillared clays, which, together with the experimental studies on the adsorption behavior of HCFC-22 in other matrices such as a 5-Å molecular sieve,[23] zeolites,[24] and MgO,[25] can provide useful information for developing new materials for HCFC-22 removal. This paper is organized as follows: (1) the morphology of the pillared clay model is illustrated, (2) the molecular potential models and the treatment of the long-range dipolar interaction are discussed, (3) details of the simulation and quantum mechanics calculation procedures are briefly outlined, (4) the discussion and analysis of the results are presented, and (5) the conclusions are summarized.

Morphology of Pillared Clays

In our simulation, the model described by Yi et al.[26] with uniform distribution of pillars between two solid walls is used to represent the pillared clay. The pillars are represented by rigid chains consisting of a given number of Lennard–Jones type spheres with the size parameter σ_{pp}. They are intercalated vertically in the space between the solid walls. Defining the direction perpendicular to the solid walls as the z-direction, the z-coordinate of the centers of the end spheres of the pillar chains is $0.5(\sigma_{pp} + \sigma_{ww})$, where σ_{ww} is the size parameter of the atoms distributed in the solid walls. Pore width H is the separation between the solid walls, which is defined by the pillar height $H = h\sigma_{pp}$, where h is the number of atoms composing one pillar chain. A schematic diagram of the pillared clay with pore width $H = 4\sigma_{pp}$ is shown in Figure 1a. The porosity of this system ψ is defined as the volume fraction of this system unoccupied by the pillars, which is given by

$$\psi = 1 - (N_{pp}\pi\sigma_{pp}^2/6A) \tag{1}$$

where N_{pp} is the number of pillars inside a $L\times\ L\times\ h\sigma_{pp}$ unit cell, A is the surface area of pore wall (x–y plane; see Figure 1a) in the simulation unit cell, and $A = L\times\ L$.

Representation of Models

Potential models

Because HCFC-22 is a simple polar fluid, the Stockmayer potential model is used to describe the intermolecular interaction of the fluid ϕ_{ff}. In our simulations, we use the effective Stockmayer potential parameters proposed by Gao et al.,[27] which are presented in Table 1. To validate these parameters, the vapor–liquid existence curve of HCFC-22 was simulated by the Gibbs ensemble Monte Carlo (GEMC) method.[28] The simulated results and the experimental data[29] are shown in Figure 2, which indicates clearly that these parameters work very well for the HCFC-22 molecules.

The Lennard–Jones potential is used to calculate the interaction ϕ_{fp} between the fluid molecule and spheres that constitute the pillars. The interaction ϕ_{pore} between a fluid molecule and a single solid pore wall is given by the well-known 10-4-3 potential.[30,31]

Activated sites, which are embedded in the interior surface

Table 1. Potential Parameters for HCFC-22, Pillar, and Solid Wall of the Pillared Clay Used in This Work

HCFC-22*			Pillar**		Solid wall†		Activated site††	
σ_{ff} (m)	ε_{ff}/k (K)	μ*	σ_{PP} (m)	ε_{PP}/k (K)	σ_{ww} (m)	ε_{ww}/k (K)	σ_{ss} (m)	ε_{ss}/k (K)
4.374×10^{-10}	199.8	1.768	3.4×10^{-10}	28.0	3.4×10^{-10}	28.0	2.187×10^{-10}	3600.0

Data from Gao et al.[27]
**Data from Cao and Wang.[11]
†Data from Steel[30] and Yang and Zhong.[31]
††Data from Jin and Wang[13] and Muller et al.[32]

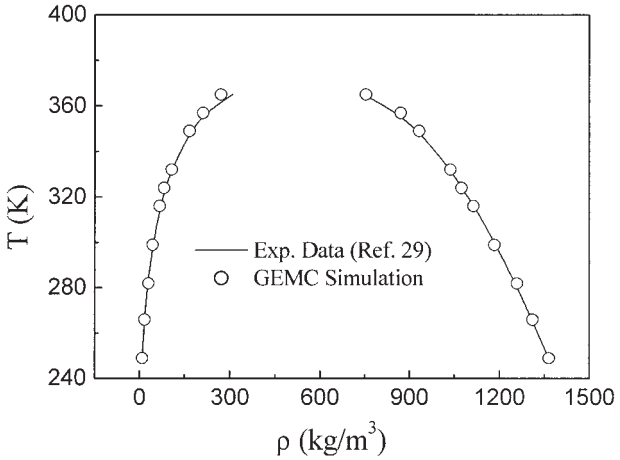

Figure 2. Vapor–liquid coexistence curve of HCFC-22.

of the solid walls, are introduced here to characterize the surface chemistry of the adsorbent. Introducing the method of Jin and Wang,[13] the activated sites are described by the Lennard–Jones potential with the same size and energy parameters used by Muller et al.[32] All of the size and energy parameters for the solid wall, the pillar, and the activated site are also shown in Table 1. In our simulations, we use the cut-and-shifted model to calculate all the Lennard–Jones potentials, and the cutoff radius $r_c = 0.5L$. All of the cross-potential parameters are determined by the Lorentz–Berthelot combining rules.

To investigate the influence of the density of activated sites, the sites are distributed in a regular array spanning the surface of solid wall with four different densities, $d_s = 0.00 \times 10^{18}$, 1.04×10^{18}, 1.42×10^{18}, and 1.86×10^{18} sites/m^2. In addition, 20% defects of the activated sites are randomly generated to describe the heterogeneity of the solid walls. Therefore the densities of the true activated sites are 0.00×10^{18}, 0.83×10^{18}, 1.14×10^{18}, and 1.49×10^{18} sites/m^2, respectively.

The total potential energy is the sum of the interaction energies of fluid–fluid, fluid–wall, fluid–pillar, and fluid-activated sites, and can then be expressed by

$$\phi_{total} = \sum_{i=1}^{N_f-1} \sum_{j=i+1}^{N_f} \phi_{ff}(\boldsymbol{r}_{ij}, \boldsymbol{\mu}_i, \boldsymbol{\mu}_j) + \sum_{i=1}^{N_f} [\phi_{pore}(z_i) + \phi_{pore}(H + \sigma_w - z_i)] + \sum_{i=1}^{N_f} \sum_{k=1}^{N_{pp}} \phi_{fp}(\boldsymbol{r}_{ik}) + \sum_{i=1}^{N_f} \sum_{k=1}^{N_{ss}} \phi_{fs}(\boldsymbol{r}_{ik}) \quad (2)$$

where N_f is the number of fluid molecules confined in pillared clays, N_{ss} is the number of activated sites, $\boldsymbol{r}$ is the position vector, $\boldsymbol{\mu}$ is the dipole moment, and z is the normal distance from the center of a fluid molecule to one of the solid wall.

Treatment of the long-range dipole–dipole interactions

In computer simulations of polar systems, an accurate and efficient treatment of long-range electrostatic interactions is of great importance. For the dipole–dipole interactions in slab geometrical systems, such as slitlike activated carbon and pillared clay, which are 3D systems with two-dimensional (2D) periodicity, the traditional Ewald summation (EW3D) method[28] cannot be used directly because there is no periodicity in one of the three dimensions (z-direction in this paper). Therefore, we used a modified version of the accurate two-dimensional Ewald type summation (EW2DM) method proposed by Grzybowski and Brodka[33] in this work.

Details of Simulation Procedure

By applying the classical GCMC technique, the details of which can be found elsewhere,[28] the adsorption behavior of HCFC-22 in pillared clays was investigated. For each state point, GCMC simulation consists of 1×10^7 steps to guarantee equilibration followed by 1×10^7 steps to sample the desired thermodynamic properties. In our simulations, the periodic boundary conditions and minimum image conventions are imposed in the x and y directions paralleling the solid walls (see Figure 1a), where the z-direction is normal to the solid walls. The surface area, A, of the square solid wall is set to $180\sigma_{ff}^2$. The initial configuration for the simulation of each isotherm is generated by randomly placing several molecules into the simulation unit cell, which should also ensure that these molecules do not overlap each other as well as with the solid walls and pillars. For subsequent points on this isotherm, the final configuration of the previous state point is used as its initial configuration.

In the grand canonical Monte Carlo method, the change in the orientation of one HCFC-22 molecule is achieved by the method of Barker and Watts.[34] The extent of the attempted displacements (including translation and rotation) is adjusted throughout the simulations so that approximately half of attempted displacements are accepted. In our simulations, all variables are reduced with respect to the Lennard–Jones parameters of HCFC-22, which are defined by

$$\mu_c^* = \mu_c/\varepsilon_{ff} \qquad T^* = kT/\varepsilon_{ff} \qquad z^* = z/\sigma_{ff} \qquad H^* = h\sigma_{pp}/\sigma_{ff}$$

$$\rho^* = \rho\sigma_{ff}^3 \qquad A^* = A/\sigma_{ff}^2 \qquad \mu^* = (\mu_{eff}^2/4\pi\varepsilon_0\varepsilon_{ff}\sigma_{ff}^3)^{1/2} \quad (3)$$

where the asterisk denotes reduced quantity; μ_c is the configurational chemical potential; k is the Boltzmann constant; ρ is the number density of the fluid; and μ_{eff} is the effective dipole moment.

Quantum Mechanics Calculations

Because HCFC-22 is modeled by Stockmayer potential, a one-site spherical potential model, the dipole moment given by this potential cannot be related to the atomic structure of the HCFC-22 molecule. Therefore, it is difficult to describe the detailed microstructure of HCFC-22 molecules in pillared clays by molecular simulations. As a result, quantum mechanics calculations were performed to determine the orientation of the dipole moment in the HCFC-22 molecule. This information, combined with the molecular simulation results of the dipolar moment distribution, was used to study the orientation of HCFC-22 molecules adsorbed on pillared clay walls. After a test of several methods, the B3LYP/6-311++G(3df, 3dp) method was adopted. B3LYP is the three-parameter hybrid functional of Becke using the Lee–Yang–Parr correlation functional, which uses the nonlocal correlation provided by the

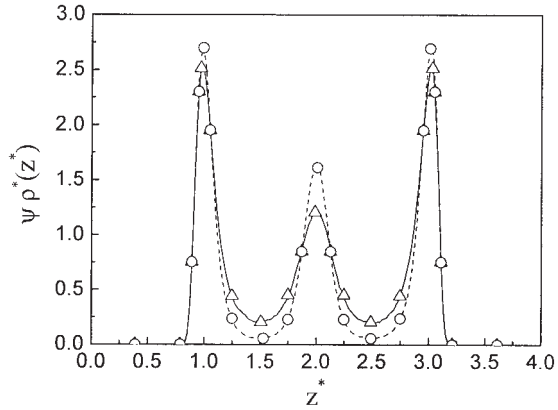

Figure 3. Comparison of the molecular local density profiles of this work with those of Yi et al.[26] This work: ψ = 1.0 (solid curve) and ψ = 0.896 (dashed curve); Yi et al.: ψ = 1.0 (triangle points) and ψ = 0.896 (open circles).

LYP expression, and VWN functional III for local correlation. The basis set 6-311++G(3df, 3pd) is a large basis set that imposes 3d functions and 1f function on nonhydrogens, and 3p functions and 1d function on hydrogens, as well as diffuse functions on all the atoms. The B3LYP/6-311++G(3df, 3dp) method is a commonly used density functional theory (DFT) method. To verify the simulation results on the microstructure of HCFC-22 molecules adsorbed in pillared clays, ab initio calculations at the level of MP2/6-31G* were further carried out. MP2 is the second-order Møller–Plesset method, which is a commonly used ab initio method. The atomic basis set 6-31G* that we use is constructed by the addition of a set of six second-order (d-type) Gaussian primitives to the split valence. MP2/6-31G* is a high-level ab initio calculation method, which was used to determine the adsorption site of a HCFC-22 molecule adsorbed on pillared clay walls. All the DFT and ab initio calculations were performed using the Gaussian 03 suite of programs,[35] and details of the calculation methods are provided in Frisch et al.[35]

Results and Discussion

Verification of the GCMC simulation program

To check our GCMC simulation program for adsorption, it was used to simulate the adsorption of a model fluid in pillared clays with pore width $H = 4\sigma_{pp}$ and two porosities, $\psi = 1.000$ (slit pore) and $\psi = 0.896$, at reduced temperature $T^* = 1.2$, which were previously studied by Yi et al.[26] using molecular dynamics simulations. To make a comparison with their results, the potential parameters specified by Yi et al. were used in our simulations; the simulated local density profiles of this work and those of Yi et al. at the overall average reduced density $\rho^* = 0.45$ are shown in Figure 3. Obviously, Figure 3 indicates that our simulation results are in good agreement with their results at the two different porosities.

Relationship between the configurational chemical potential and bulk pressure for HCFC-22 at 300 K

The GCMC simulations for adsorption are carried out at a fixed slit width H, temperature T, and configurational chemical potential $\mu_{con.}$ However, pressure is more visible and convenient, and the adsorption isotherms are measured using temperature and pressure as independent variables. Therefore, a relationship between bulk pressure P and μ_{con} is necessary, which is obtained by direct GCMC simulation of the PVT behavior of the bulk fluid of HCFC-22 at 300 K, and the EW3D method with a so-called tin-foil boundary condition[36] is used to handle the long-range dipole–dipole interactions.

The GCMC simulated results are shown in Figure 4. During the simulation, the volume of the simulation unit cell is adjusted to ensure that enough molecules are retained in it for satisfactory accuracy. Through the curve in Figure 4, an analytical expression for the relationship between the reduced chemical potential and the bulk pressure is proposed as follows

$$\mu_c^* = -6.0660 + 1.4378 \ln\left(\frac{P}{1\ \text{MPa}}\right) \quad (P < 1.20\ \text{MPa}) \quad (4)$$

where the pressure is in MPa.

Adsorption of HCFC-22 in pillared clays

The pore width is one of the main characteristic parameters for pillared clays. Figures 5a–c show the dependency of excess adsorption amount Γ_{ex} at $T = 300$ K on the pore width of pillared clays with three porosities ψ at eight reduced pressures P/P_s, where the saturated vapor pressure P_s of HCFC-22 at $T = 300$ K is taken as 1.1004 MPa.[29] The excess adsorption amount Γ_{ex} is calculated by

$$\Gamma_{ex} = (\rho^* - \rho^*_{bulk})/(N_a\sigma_{ff}^3) \quad (5)$$

where ρ^*_{bulk} is the reduced density of bulk fluid at the same temperature and chemical potential (or pressure) as those of ρ^*, which can be obtained directly by GCMC simulation of bulk fluid; and N_a is the Avogadro constant.

As can be seen from Figures 5a–5c, for all of the three porosities, $H = 4\sigma_{pp}$ (corresponding to $H = 1.36 \times 10^{-9}$ m) is the optimal pore width for the adsorption of HCFC-22 in pillared clays. Figure 5a also shows that in pillared clays with porosity $\psi = 1.000$ (that is, slitlike graphite), for pore width $H = 3\sigma_{pp}$, there is a very small adsorption amount at reduced

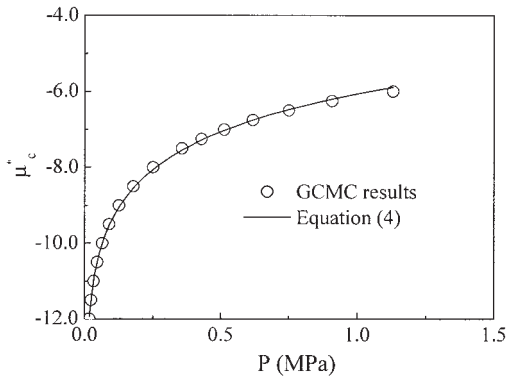

Figure 4. GCMC results for the relationship between the configurational chemical potential and bulk pressure for HCFC-22 at T = 300 K.

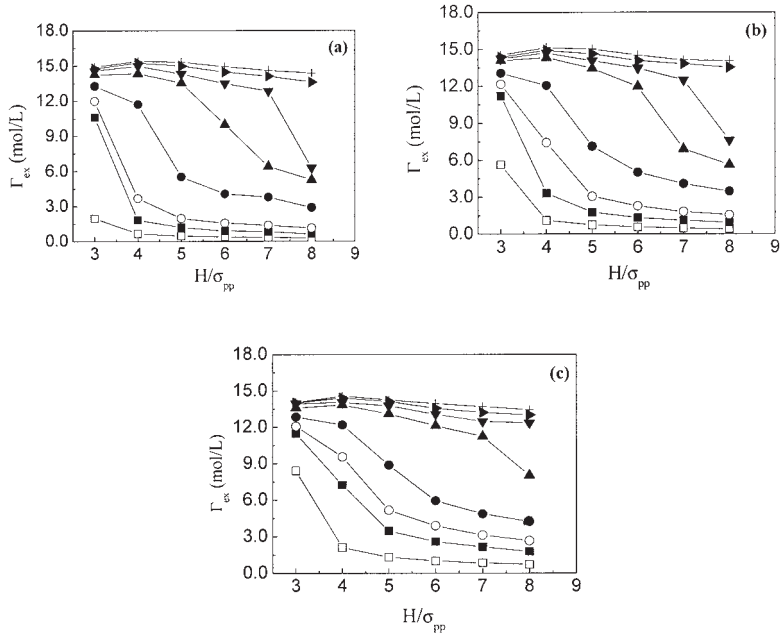

Figure 5. Dependency of excess adsorption amount Γ_{ex} in pillared clays with different porosities.

(a) $\psi = 1.000$; (b) $\psi = 0.984$; (c) $\psi = 0.956$, on pore width at various reduced pressures P/P_s: □, 0.02; ■, 0.03; ○, 0.04; ●, 0.08; ▲, 0.23; ▼, 0.32; ▶, 0.47 + 0.68.

pressure $P/P_s = 0.02$, whereas a significantly large increase is observed as the reduced pressure is somewhat increased to 0.03, which is the representative feature of the micropore filling effect.

The porosity ψ is another important parameter that controls both adsorption and diffusion behaviors of fluid in pillared clays. For the pillared clay with the optimal pore width $H = 1.36 \times 10^{-9}$ m, the relationship between the excess adsorption amount Γ_{ex} at $T = 300$ K and the porosity is shown in Figure 6, where the excess adsorption amount is expressed as a function of the reduced pressure. It is found in Figure 6 that for the pillared clay with the four simulated porosities, all the adsorption behaviors at such pore width also exhibit the feature of micropore filling effect. Figure 6 also shows that at low reduced pressures, the excess adsorption amount increases monotonically with decreasing porosity, which can be attributed to the contribution of the additional adsorption surface provided by pillars. However, at high reduced pressures, an inverse trend was observed, that is, the larger the porosity, the greater the excess adsorption amount, which is explained by the accessible volume of the system that is the dominating factor compared with the adsorption contributions of the pillars. Yi et al.[8] also observed these different adsorption patterns for adsorption of the model Lennard–Jones fluid in pillared clays. Furthermore, we can also see from Figure 6 that the reduced pressure for the saturated adsorption is a monotonically increasing function of the porosity. In addition, Figure 6 also shows that the maximum adsorption for all of the porosities ψ occurs at the reduced adsorption pressure of around $P/P_s = 0.39$.

The effect of porosity of the pillared clay on the excess adsorption amount Γ_{ex}, with pore width $H = 2.38 \times 10^{-9}$ m at $T = 300$ K, is shown as a function of reduced pressure in Figure 7. The adsorption behaviors are similar to those in the pillared clay with pore width $H = 1.36 \times 10^{-9}$ m. What should be noted is that capillary condensation begins to occur in this pore width, and the corresponding reduced pressure increases with increasing porosity.

Figure 8 shows the effect of the density of activated sites on the excess adsorption amount Γ_{ex} in the pillared clay with pore width $H = 1.36 \times 10^{-9}$ m and porosity $\psi = 0.956$. It is observed from Figure 8 that the pillared clay without activated sites needs the highest pressure for saturation adsorption because of its natural physical adsorption, whereas the density $d_s = 1.49 \times 10^{18}$ sites/m^2 of the pillared clay with the largest activated sites shows the greatest excess adsorption amount through all the simulated pressures, resulting from the addi-

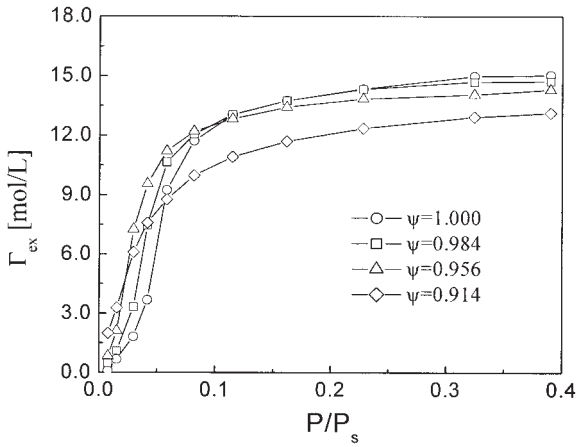

Figure 6. Relationship between the excess adsorption amount Γ_{ex} at $T = 300$ K and the porosity of the pillared clay with pore width $H = 1.36 \times 10^{-9}$ m.

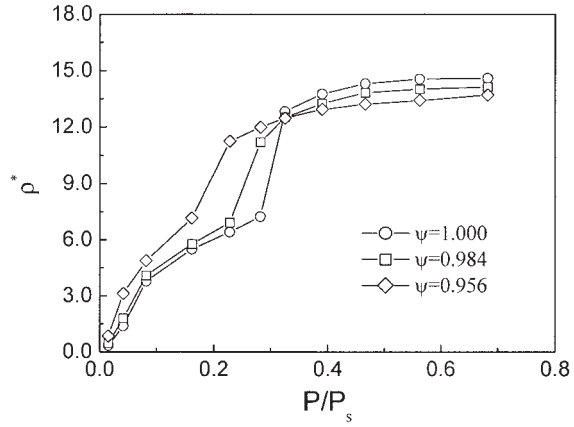

Figure 7. Relationship between the excess adsorption amount Γ_{ex} at T = 300 K and the porosity of pillared clay.

Pore width $H = 2.38 \times 10^{-9}$ m.

tional chemical adsorption contributions of the activated sites. However, the difference of the excess adsorption amounts becomes smaller at higher activated site densities because of the space limitation of the pillared clay. This can be seen from the almost comparable adsorption amounts between the two densities of $d_s = 1.14 \times 10^{18}$ and 1.49×10^{18} sites/m^2 shown in Figure 8.

Microstructure of HCFC-22 in pillared clays

The Local Density Profile ρ(z*) for Center of Mass.* The local density profile $\rho^*(z^*)$ for center of mass is calculated by the following equation

$$\rho^*(z^*) = \langle dN(z^*)\rangle/(A^* \cdot \Psi \cdot \Delta z^*) \qquad (6)$$

where $\langle dN(z^*)\rangle$ is the ensemble average of the number of adsorbed molecules in a layer located in z^* to $z^* + \Delta z^*$, and the denominator is the reduced accessible volume of this layer. Here, Δz^* takes a value of $0.005H^*$.

Figures 9a–l show the effect of the simulated reduced pressure on the local density profiles for center of mass of HCFC-22 in pillared clays with pore width $H = 1.36 \times 10^{-9}$ m at T = 300 K. It is found that all the pillared clays in the three porosities can accommodate three adsorbed layers with two contact layers adjacent to the walls and one inner layer. At very low pressure of $P/P_s = 0.02$, the peak of the contact layer increases with decreasing porosity, attributed to the contributions of the pillars to the adsorption (see Figures 9a–c), and the inner layer appears only in the pillared clay with porosity ψ = 0.914. Further increases of reduced pressure lead to the appearance of three layers for all three porosities, and the difference among the pillared clays becomes smaller. At high pressure, the peaks of the contact layers increase slightly with decreasing porosity, whereas the peak of the inner layer shows the opposite trend. This is consistent with the fact that there are two main factors that affect the adsorption capability of pillared clays without activated sites: the amount of available surface and the available volume. At low pressure, physical adsorption is the main force for adsorption, and thus the amount of available surface is predominant, whereas at high pressure, the available volume becomes more significant.

Figures 10a–l compare the effects of the density of the activated sites and the adsorption pressure on the local density profiles of HCFC-22 in pillared clays with pore width $H = 1.36 \times 10^{-9}$ m and porosity $\psi = 0.956$. At very low reduced pressure of $P/P_s = 0.01$, the pillared clay with no activated sites ($d_s = 0.00 \times 10^{18}$ sites/m^2) exhibits only weak physical adsorption, whereas the local densities of contact layers adjacent to the walls in the pillared clay with $d_s = 0.83 \times 10^{18}$ and 1.49×10^{18} sites/m^2 are much higher. This indicates that the chemical adsorption contributes substantially to the adsorption at low pressure. However, when the pressure is increased, the difference among the clays with different densities of the activated sites becomes smaller, which is explained by the fact that at high pressure the available volume is the predominant factor affecting the adsorption capability.

The Orientation Distribution of Dipole Moment ρ(z*, θ) and the Orientation of HCFC-22 Adsorbed in Pillared Clays.* The orientation distribution of dipole moment $\rho^*(z^*, \theta)$ is another property used to describe the microstructure of HCFC-22 in pillared clays, which is given by[37]

$$\rho^*(z^*, \theta) = \langle dN(z^*, \theta)\rangle/(A^* dz^* d\theta \sin\theta) \qquad (7)$$

where θ is the angle between the vector of dipole moment and the z-axis. $\langle dN(z^*, \theta)\rangle$ is the ensemble average of the number of adsorbate molecules for which centers of mass locate at the layer z^* to $z^* + \Delta z^*$ and angles lie in the range θ to $\theta + \Delta\theta$. For dipole molecules, angle θ should be in $0 \le \theta \le \pi$. $\theta = 0$ and π indicate that the dipole moment has a perpendicular orientation to the pore wall, whereas $\theta = \pi/2$ corresponds to parallel orientation. Angle θ is divided into 40 slices with angle interval $\Delta\theta = \pi/40$.

To investigate the orientation distribution of the dipole moments of HCFC-22 molecules adsorbed in pillared clays, it is essential to know the orientation of the dipole moment in the HCFC-22 molecule. Thus, the Gaussian 03 suite of programs[35]

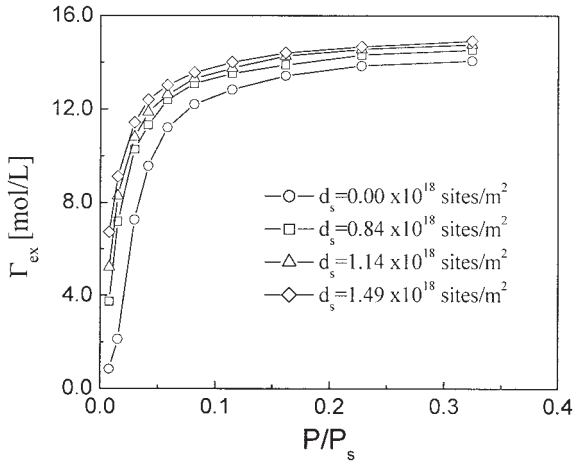

Figure 8. Effect of the density of the activated sites on the excess adsorption amount Γ_{ex} in pillared clay.

Pore width $H = 1.36 \times 10^{-9}$ m and porosity $\psi = 0.956$ at T = 300 K.

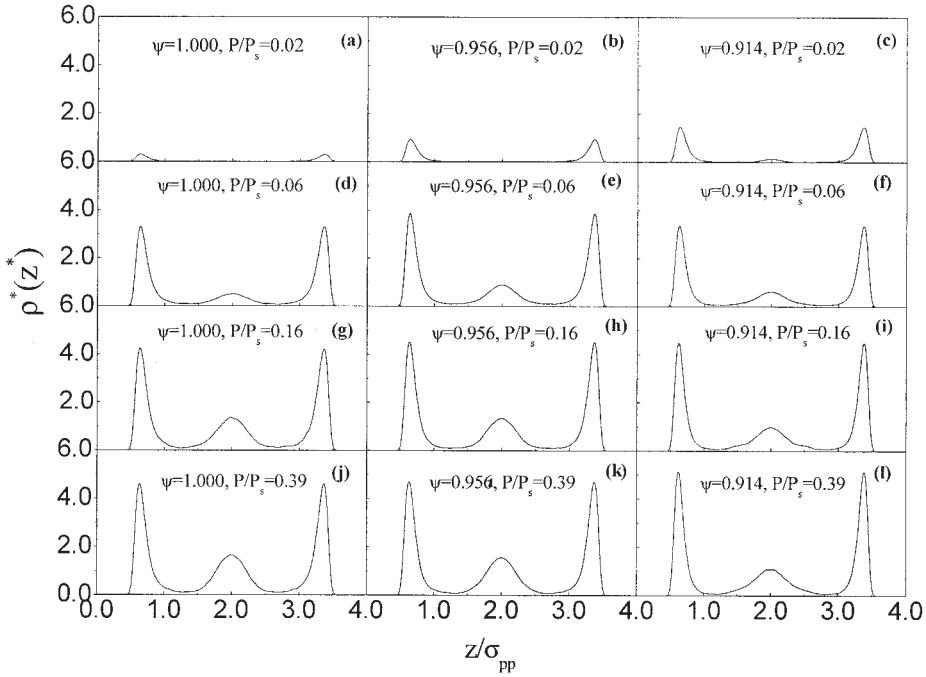

Figure 9. Effects of porosity and adsorption pressure on the local density profiles for center of mass of HCFC-22 in pillared clay.

Pore width $H = 1.36 \times 10^{-9}$ m at $T = 300$ K.

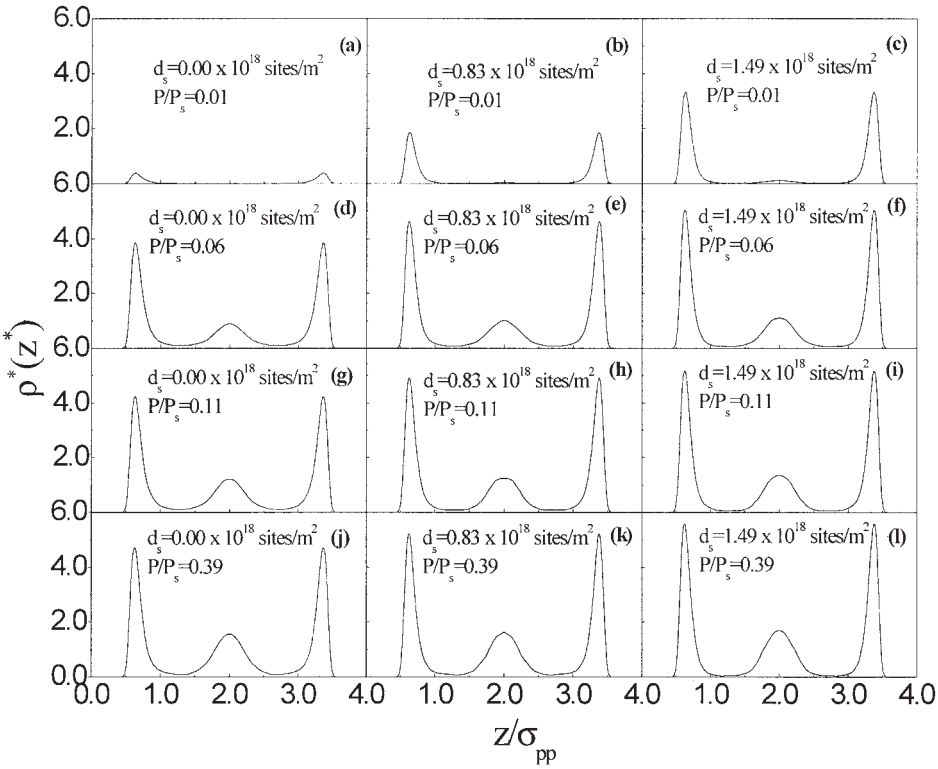

Figure 10. Effects of the density of the activated sites and adsorption pressure on the local density profiles for center of mass of HCFC-22 in pillared clay.

Pore width $H = 1.36 \times 10^{-9}$ m and porosity $\psi = 0.956$ at $T = 300$ K.

Table 2. Comparison of the Calculated Molecular Geometric Parameters and the Dipole Moment for HCFC-22 with the Experimental Results

	Quantum Calculation	Experiment*
Bond length (m)		
C—H	1.09×10^{-10}	1.08×10^{-10}
C—F	1.34×10^{-10}	1.35×10^{-10}
C—Cl	1.78×10^{-10}	1.76×10^{-10}
Bond angle (degree)		
H—C—F	110.1	108.3
H—C—Cl	109.1	107.8
F—C—F	108.2	107.7
F—C—Cl	109.7	109.5
Dipole moment (C · m)		
μ_{ff}	4.87×10^{-30}	(4.87×10^{-30})**

Data from Hall et al.[38]
**Data from Nelson et al.[39]

is used to perform ab initio and DFT calculations on HCFC-22 molecules. Various methods have been tested and the results using density functional theory at the level of B3LYP/6-311++G(3df, 3dp) are in best agreement with the experimental values both for the molecular geometric parameters[38] and the dipole moment,[39] as shown in Table 2. The calculated results show that the orientation of the dipole moment in HCFC-22 molecule is located in the plane formed by atoms C, H, and Cl. The vector of dipole moment lies between the bond vectors C → Cl and C → H, and forms an 6.2° angle with bond vector C → H. Because the angle between bond vectors C → Cl and C → H is 109.1°, the vector of the dipole moment is much closer to the bond vector C → H and we can even treat the two vectors as identical in direction. Two F atoms are symmetrically distributed in the two sides of the plane formed by atoms C, H, and Cl. The diagrammatic representation of the orientation of dipole moment $\boldsymbol{\mu}$ in the HCFC-22 molecule is shown in Figure 1b.

The orientation distributions $\rho^*(z, \theta)$ of dipole moments of HCFC-22 molecules adsorbed in pillared clays, with pore width $H = 1.36 \times 10^{-9}$ m at pressure $P/P_s = 0.01$ and $T = 300$ K for two porosities, are shown in Figure 11. Because of the symmetry of pillared clays along the z-direction, only orientation distributions in half of the pore width are shown. The simulated results demonstrate that most of the dipole moments orient perpendicularly to the walls (that is, most of the HCFC-22 molecules orient perpendicularly to the walls in the direction of C → H), indicating that the hydrogen atom is the adsorption site of a HCFC-22 molecule adsorbed on the walls at low pressure when physical adsorption is the main driving force.

To verify this conclusion, we further performed quantum mechanics calculations to study the orientation of a HCFC-22 molecule adsorbed on graphite surface at low pressure at a higher level. In the calculations, a one-layer graphite model ($C_{16}H_{10}$) was used, in which the C—C bond length was taken as 1.420×10^{-10} m with the boundary of the model being saturated with hydrogen atoms.[40] The structure for the HCFC-22 molecule was taken as obtained in this work using the B3LYP/6-311++G(3df, 3dp) method. Three paths were examined for a HCFC-22 molecule that approaches the graphite layer, that is, the approaching atom is hydrogen, fluorine, and chlorine, respectively. The ab initio calculated results at the level of MP2/6-31G* show that the lowest energy is obtained when the hydrogen atom is adsorbed with the carbon atom on the graphite layer, as shown in Figure 12, leading to the conclusion that the hydrogen atom in the HCFC-22 molecule is the adsorption site with the graphite wall. This is consistent with what we have obtained by molecular simulations. Therefore, the ab initio study combined with the molecular simulation results can clearly indicate the orientation of HCFC-22 molecules adsorbed in pillared clays as well as the orientation distributions of dipole moments of HCFC-22 molecules.

To further study the effects of pressure, the orientation distributions $\rho^*(z, \theta)$ of dipole moments of HCFC-22 molecules adsorbed in pillared clays at high reduced pressure, $P/P_s = 0.39$, were simulated, as shown in Figure 13a for porosity $\psi = 1.000$ and in Figure 13b for $\psi = 0.956$, respectively. For both porosities, in contrast with that at low pressure, most of the dipole moments of the molecules in the contact layers orient parallel to the wall, whereas the dipole moments of the molecules in the inner layer orient randomly for porosity $\psi = 1.000$ (see Figure 13a) and preferentially perpendicular to the walls for porosity $\psi = 0.956$ (see Figure 13b). This may be explained by the fact that at high pressure a packing effect is the predominant factor that determines the orientation of HCFC-22 molecules in pillared clays. Therefore, this work demonstrates that the orientation of HCFC-22 molecules adsorbed in pillared clays changes with pressure, preferentially perpendicular to the walls in the direction of C → H at low pressure with hydrogen atoms as adsorption sites, and with most of the dipole moments being parallel to the walls at high pressure.

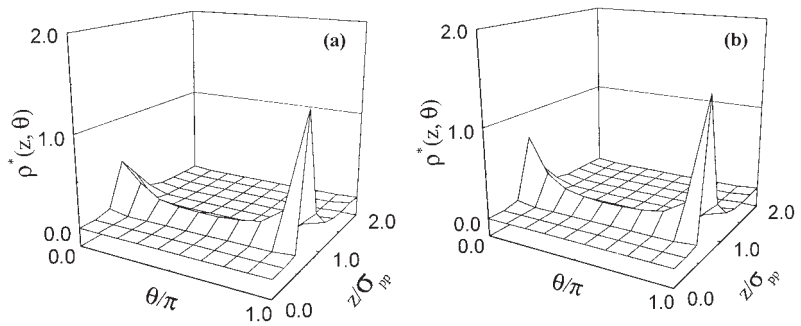

Figure 11. Orientation distributions of dipole moments of HCFC-22 molecules adsorbed in pillared clays.
Pore width $H = 1.36 \times 10^{-9}$ m at reduced pressure $P/P_s = 0.01$ and $T = 300$ K. (a) $\psi = 1.000$; (b) $\psi = 0.956$.

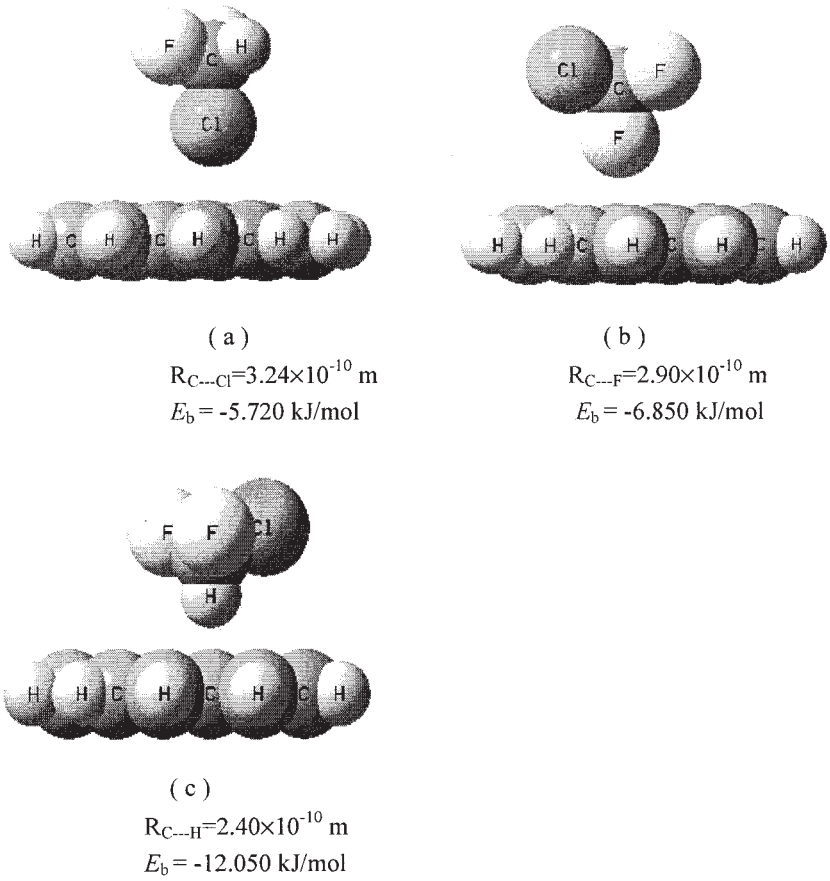

Figure 12. Structure and binding energy of HCFC-22 adsorbed on one-layer graphite model $C_{16}H_{10}$ calculated with the MP2/6-31G* method.

Conclusions

In this work, GCMC simulations combined with quantum mechanics calculations were used to study the adsorption and microstructure of HCFC-22 in pillared clays. The simulation results show that, at $T = 300$ K, the optimal pore width and reduced adsorption pressure for the maximum adsorption are $H = 1.36 \times 10^{-9}$ m and $P/P_s = 0.39$ K, respectively. At low pressures, the excess adsorption amount decreases monotonically with increasing porosity, whereas at high pressures, the inverse trend was obtained. The simulation results also demonstrate that the effect of the density of activated sites on the adsorption isotherms is significant at low pressures, which becomes weaker at high pressures.

The orientation of dipole moment in the HCFC-22 molecule was determined using the B3LYP/6-311++G(3df, 3dp) method, which was incorporated into the molecular simulations to study the orientation distributions of dipole moment of HCFC-22. In addition, the adsorption site of the HCFC-22 molecules with the pillared clay walls was determined by use of the MP2/6-31G* method. A combination of the results from the molecular simulations and the quantum mechanics calculations clearly demonstrates that the hydrogen atom is the

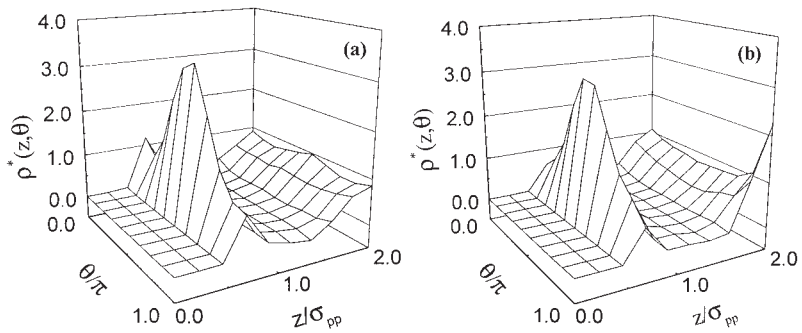

Figure 13. Orientation distributions of dipole moments of HCFC-22 molecules adsorbed in pillared clays.

Pore width $H = 1.36 \times 10^{-9}$ m at reduced pressure $P/P_s = 0.39$ and $T = 300$ K. (a) $\psi = 1.000$; (b) $\psi = 0.956$.

adsorption site in a HCFC-22 molecule adsorbed on a graphite surface, and most of the HCFC-22 molecules in contact layers are in perpendicular orientation to the walls in the direction of C → H at low pressures, where the physical adsorption is the predominant driving force. At high pressures, the packing effect becomes predominant and most of the HCFC-22 molecules are in parallel orientation to the walls in the direction of C → H. This work shows that a combination of molecular simulation and quantum mechanics calculations can reveal the details of the adsorption and microstructure of HCFC-22 molecules confined in pillared clays, providing deep insight into the adsorption mechanisms, which proves to be very useful in the development of recovery processes for HCFC-22 molecules as well as for the porous material design and development. In addition, the present work shows that pillared clays have higher adsorption capability than that of activated carbons for HCFC-22 at ambient pressure, which may be a promising material for HCFC-22 removal. However, the practical usefulness of pillared clays as HCFC-22 removal materials needs to be proved by experimental investigations.

Acknowledgments

The financial support of the Teaching and Research Award Program for Outstanding Young Teachers in Higher Education Institutions of the Ministry of Education (MOE), China, and the Trans-Century Training Programme Foundation for the Talents by the MOE, China, is greatly appreciated. We are also very grateful to Prof. Aleksander Bródka for his help and the code for the EW2DM calculation.

Literature Cited

1. Devotta S, Waghmare AV, Sawant NN, Domkundwar BM. Alternatives to HCFC-22 for air conditioners. *Applied Thermal Engineering.* 2001;21:703-715.
2. Tsai WT. A review of environmental hazards and adsorption recovery of cleaning solvent hydrochlorofluorocarbons (HCFCs). *Journal of Loss Prevention in the Process Industries.* 2002;15:147-157.
3. Baksh MS, Yang RT. Unique adsorption properties and potential energy profiles of microporous pillared clays. *AIChE Journal.* 1992; 38:1357-1368.
4. Pereiara PR, Pires J, Brotas de Carvalho M. Zirconium pillared clays for carbon dioxide/methane separation. 1. Preparation of adsorbent materials and pure gas adsorption. *Langmuir.* 1998;14:4584-4588.
5. Smit B, Siepmann JI. Simulating the adsorption of alkanes in zeolites. *Science.* 1994;264:1118-1120.
6. Koga K, Tanaka H, Zeng XC. First-order transition in confined water between high-density liquid and low-density amorphous phases. *Nature.* 2000;408:564-567.
7. Cracknell R, Koh CA, Thompson SM, Gubbins KE. Molecular simulation of adsorption simple gases in aluminophosphates and pillared clays. *Materials Research Society Symposium Proceedings.* 1993;290: 135-143.
8. Yi XH, Shing KS, Sahimi M. Molecular simulation of adsorption and diffusion in pillared clays. *Chemical Engineering Science.* 1996;51: 3409-3426.
9. Yi XH, Ghassemzadeh J, Shing KS, Sahimi M. Molecular dynamics simulation of gas mixtures in porous media. I. Adsorption. *Journal of Chemical Physics.* 1998;108:2178-2188.
10. Ghassemzadeh J, Xu LF, Tsotsis TT, Sahimi M. Statistical mechanics and molecular simulation of adsorption in microporous materials: Pillared clays and carbon molecular sieve membranes. *Journal of Physical Chemistry B*. 2000;104:3892-3905.
11. Cao DP, Wang WC. Computer simulation of adsorption of CCl_4 in activated carbon and layered pillared materials at ambient temperature. *Physical Chemistry Chemical Physics.* 2002;4:3720-3726.
12. Maddox M, Ulberg D, Gubbins KE. Molecular simulation of simple fluids and water in porous carbons. *Fluid Phase Equilibria.* 1995;104: 145-158.
13. Jin WZ, Wang WC. Computer simulation of adsorption of a Stockmayer molecule chlorodifluoromethane in activated carbon slit pores. *Journal of Chemical Physics.* 2001;114:10163-10169.
14. Volpe M, Cleri F. Role of surface chemistry in hydrogen adsorption in single-wall carbon nanotubes. *Chemical Physics Letters.* 2003;371: 476-482.
15. Smith MR Jr, Bittner EW, Shi W, Johnson JK, Bockrath BC. Chemical activation of single-walled carbon nanotubes for hydrogen adsorption. *Journal of Physical Chemistry B.* 2003;107:3752-3760.
16. Malla PB, Yamanaka S, Komarneni S. Unusual water vapor adsorption behavior montmorillonite pillared with ceramic oxides. *Solid State Ionics*. 1989;32–33:354-362.
17. Yamanaka S, Malla PB, Komarneni S. Water adsorption properties of alumina pillared clay. *Journal of Colloid and Interface Science.* 1990; 134:51-58.
18. Zhu HY, Gao WH, Vansant EF. The porosity and water adsorption of alumina pillared montmorillonite. *Journal of Colloid and Interface Science*. 1995;171:377-385.
19. Sychev M, Prikhod'ko R, Stepanenko A, Rozwadowski M, de Beer VHJ, van Santen RA. Characterisation of the microporosity of chromia- and titania-pillared montmorillonties differing in pillar density. II. Adsorption of benzene and water. *Microporous and Mesoporous Materials.* 2001;47:311-321.
20. Delville A, Sokołowski S. Adsorption of water vapor on montmorillonite: Computer simulation studies. *Journal of Physical Chemistry.* 1993;97:6261-6271.
21. Hesen EJM, Tambach TJ, Bliek A, Smit B. Adsorption isotherms of water in Li-, Na- and K- montmorillonite by molecular simulation. *Journal of Chemical Physics.* 2001;115:3322-3329.
22. Marry V, Turq P, Cartailler T, Levesque D. Microscopic simulation of structure and dynamics of water and counterions in a monohydrated montmorillonite. *Journal of Chemical Physics*. 2002;117: 3454-3463.
23. Cannon P. Reaction of chlorodifluoromethane with linde molecular sieve 5Å. *Journal of the American Chemical Society.* 1958;80:1766-1767.
24. Wylie DJ, Cooney RP, Seakins JM, Millar GJ, Spectroscopic studies of the adsorption and reactions of chlorofluorocarbons (CFC-11 and CFC-12) and hydrochlorofluorocarbon (HCFC-22) on oxide surfaces. *Vibrational Spectroscopy*. 1995;9:245-256.
25. Zakharenko VS, Parmon VN. Photoadsorption and photocatalytic processes affecting the composition of the earth's atmosphere: II. Dark and photostimulated adsorption of freon 22 (CHF_2Cl) on MgO. *Kinetics and Catalysis.* 2000;41:834-838.
26. Yi XH, Shing KS, Sahimi M. Molecular dynamics simulation of diffusion in pillared clays. *AIChE Journal.* 1995;41:456-468.
27. Gao GT, Wang WC, Zeng XC. Gibbs ensemble simulation of HCFC/HFC mixtures by effective Stockmayer potential. *Fluid Phase Equilibria*. 1999;158–160:69-78.
28. Allen MP, Tildesley DJ. *Computer Simulation of Liquid*. Oxford, UK: Oxford University Press; 1987.
29. Baehr HD, Tillner-Roth R. *Thermodynamic Properties of Environmentally Acceptable Refrigerants*. Berlin, Germany: Springer-Verlag; 1994.
30. Steel WA. The physical interaction of gases with crystal solids. I. Gas-solid energies and properties of isolated adsorbed atoms. *Surface Science.* 36:317-352 (1973).
31. Yang QY, Zhong CL. Computer simulations of adsorption characteristics of carbon dioxide in slit graphite pores. *Canadian Journal of Chemical Engineering*. in press.
32. Muller EA, Rull LF, Vega LF, Gubbins KE. Adsorption of water on activated carbons: A molecular simulation study. *Journal of Physical Chemistry.* 1996;100:1189-1196.
33. Grzybowski A, Brodka A. Computationally efficient method for summing interactions of point dipoles in three dimensions with two-dimensional periodicity. *Chemical Physics Letters.* 2002;361: 329-333.
34. Barker JA, Watts RO. Structure of water: A Monte Carlo calculation. *Chemical Physics Letters.* 1969;3:144-145.
35. Frisch MJ, Trucks GW, Schlegel HB, Scuseria GE, Robb MA, Cheeseman JR, Montgomery JA, Jr, Vreven T, Kudin KN, Burant JC, Millam JM, Iyengar SS, Tomasi J, Barone V, Mennucci B, Cossi M, Scalmani G, Rega N, Petersson GA, Nakatsuji H, Hada M, Ehara M, Toyota K, Fukuda R, Hasegawa J, Ishida M, Nakajima T, Honda Y, Kitao O,

Nakai H, Klene M, Li X, Knox JE, Hratchian HP, Cross JB, Adamo C, Jaramillo J, Gomperts R, Stratmann RE, Yazyev O, Austin AJ, Cammi R, Pomelli C, Ochterski JW, Ayala PY, Morokuma K, Voth GA, Salvador P, Dannenberg JJ, Zakrzewski VG, Dapprich S, Daniels AD, Strain MC, Farkas O, Malick DK, Rabuck AD, Raghavachari K, Foresman JB, Ortiz JV, Cui Q, Baboul AG, Clifford S, Cioslowski J, Stefanov BB, Liu G, Liashenko A, Piskorz P, Komaromi I, Martin RL, Fox DJ, Keith T, Al-Laham MA, Peng CY, Nanayakkara A, Challacombe M, Gill PMW, Johnson B, Chen W, Wong MW, Gonzalez C, Pople JA. Gaussian 03. Pittsburgh PA: Gaussian, Inc.; 2003.

36. De Leeuw SW, Perram JW, Smith ER. Computer simulation of the static dielectric constant of systems with permanent electric dipoles. *Annual Review of Physical Chemistry.* 1986;37:245-270.
37. Vishnyakov A, Piotrovskaya EM, Brodskaya EN. Monte Carlo computer simulation of adsorption of diatomic fluids in slitlike pores. *Langmuir.* 1996;12:3643-3649.
38. Hall CD, Johnson KA, Burgess AN, Winterton N, Howells WS. The structure of fluid fluoroform, chlorodifluoromethane, and dichlorodifluoromethane by neutron diffraction. *Molecular Physics.* 1991;74:27-33.
39. Nelson RD, Lide DR, Maryott AA. Selected values of electric dipole moments for molecules in the gas phase. *National Standard Reference Data Series*, National Bureau of Standards (NBS), No. 10. Washington, DC: NBS; 1967.
40. Ruuska H, Pakkanen TA. Ab initio model study on a water molecule between graphite layers. *Carbon.* 2003;41:699-706.

Manuscript received Apr. 27, 2004, and revision received May 24, 2004.